Improved Cloud Partitioning Sampling for Iterative Closest Point: Qualitative and Quantitative Comparison Study

Polycarpo Souza Neto, Nicolas S. Pereira and George A. P. Thé
Department of Teleinformatic Engineering, Federal University of Ceara, Fortaleza, Pici campus, Bl 725, Zip code 60455-970, Brazil

Keywords: Computer Vision, Iterative Closest Point, Point Cloud Registration, Point Cloud Sampling.

Abstract: In 3D reconstruction applications, an important issue is the matching of point clouds corresponding to different perspectives of a given object in a scene. Traditionally, this problem is solved by the use of the Iterative Closest point (ICP) algorithm. In view of improving the efficiency of this technique, authors recently proposed a preprocessing step which works prior to the ICP algorithm and leads to faster matching. In this work, we provide some improvements in our technique and compare it with other 4 variations of sampling methods using a RMSE metric, an Euler angles analysis and a modification structural similarity (SSIM) based metric. Our experiments have been carried out on four different models from two different databases, and revealed that our cloud partitioning approach achieved more accurate cloud matching, in shorter time than the other techniques. Finally we tested the robustness of the technique adding noise and occlusion, obtaining, as in the other tests, superior performance.

1 INTRODUCTION

Efficient 3D reconstruction of indoor and outdoor environments is a hot research topic in many areas like machine learning (Pan et al., 2017), in computer vision (Rodolà et al., 2015), in photogrammetry (Zhang and Lin, 2017) as well as for helping agriculture through the use automated system for capturing 3D data of plants and vegetation (Chaudhury et al., 2015) and robotics (Ćesić et al., 2016) for tracking and detection of elements in scenes. Also in manufacturing industry (Toro et al., 2015) it may be seen as a provider of innovative and efficient solutions for optimizing shop floor processes (Malamas et al., 2003), what has been suggested especially in cases of collision avoidance (Cigla et al., 2017) in non-structured scenarios and for safer human-machine interaction (Gorecky et al., 2014), which ultimately may speed up manufacturing processes.

In a few words, 3D reconstruction means data fusion of images from different camera perspectives and consists essentially on making partial descriptions of a scene to merge into a scene representation as a whole. In the literature, this task has been first solved by the Iterative Closest Point algorithm (Besl and McKay, 1992). It is aimed at obtaining the rigid transformation able to minimize the distance between two datasets, e.g. two acquired point clouds of a given scene, allowing an integration of images acquired from different camera position and orientation.

In general, ICP performs better when some data preprocessing is carried out. In the literature, outliers removal (Weinmann, 2016) and undersampling (Rodolà et al., 2015) are typical issues; while the former is important for good representation of the rigid transformation pursued, latter influences computational costs and its adoption is needed for several reasons, as pointed out in (Rodolà et al., 2015). The sampling methods are useful discretization step to produce data which is much easier to handle with algorithms. Even if the surface is a triangular mesh, sampling reduces the number of points to be represented, which may be required if the complexity of the task is not linear or the clouds are large in size. However, the goal of sampling is the selection of surface points that are relevant with respect to the task that is to be performed.

Authors recently proposed a sampling method named cloud-partitioning ICP (CP-ICP) and it is revisited in this work, since important changes were made to it (Pereira et al., 2015). We compared this method with ICP as well as sampling methods based on sampling. The techniques of comparison using sampling were Random and Uniform Sampling. Uni-

Neto, P., Pereira, N. and Thé, G.
Improved Cloud Partitioning Sampling for Iterative Closest Point: Qualitative and Quantitative Comparison Study.
DOI: 10.5220/0006828500490060
In *Proceedings of the 15th International Conference on Informatics in Control, Automation and Robotics (ICINCO 2018) - Volume 2*, pages 49-60
ISBN: 978-989-758-321-6

form and random sampling variants were also studied in (Rusinkiewicz and Levoy, 2001). In the case of Random Sampling, two variants were used, with sampling of 50% and 70% of the data set. We have compared the sampling methods quantitatively using root mean squared error (RMSE) and Euler angles; in addition, we adapt a form of quantitative evaluation based on multi-view analysis of the registration images, exposing these images to Structural Similarity Index Measure (SSIM), proposing in (Wang et al., 2004). Effects of adding noise and occlusion were also investigated for some models, in order to provide insight of robustness of the CP-ICP method under real conditions of data acquisition.

The ICP implementation (in C++) of the Point Cloud Library (PCL)(Holz et al., 2015) was adopted here because it is widely used as benchmark by the research community.

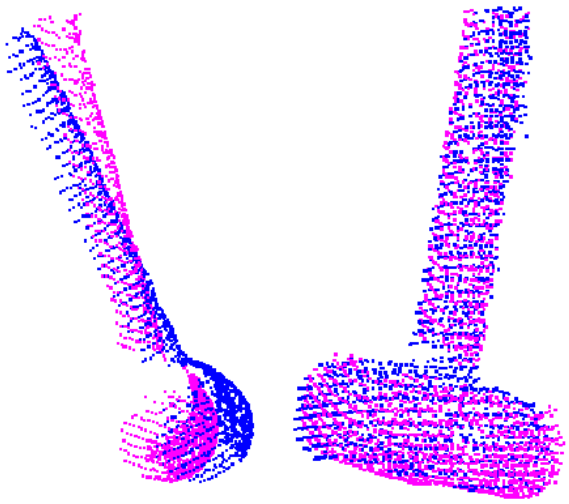

Figure 1: Point cloud of Hammer model before (left) and after(right) submited from ICP algorith (Aleotti et al., 2014).

2 BASICS OF 3D MATCHING

The ICP algorithm was proposed in (Besl and McKay, 1992) and aims at finding a transformation that optimizes a rotation and translation in two sets of data (sets of line segments, implicit curves, sets of triangles,implicit, parametric surfaces, point sets, etc.). The algorithm uses one of the data sets as reference, hereafter referred to as set and applies rotations and translations to the other set, called here from now on as input set, in order to minimize the following cost function:

$$F(\vec{q}) = \frac{1}{N}\sum_{i=1}^{N} \| \vec{x}_i - (R\vec{p}_i + T) \| \qquad (1)$$

where:

- N=number of points;
- $\vec{x}_i$ =i-th vector related to the target point cloud;
- $\vec{p}_i$ =i-th vector related to the input point cloud;
- R= rotaxion matrix obtained from ICP;
- T= translation vector obtained from ICP.

The result achieved from the ICP algorithm is the optimum rotation and translation between the two datasets. Fig. 1 illustrates what happens after applying the ICP algorithm to point clouds. In the left, the initial pose of the inputs and in the right, a successful registration between the two point clouds.

3 SAMPLINGS

3.1 Uniform Sampling

This ICP variant allows for crudely aligning one range image to another and then invoking an algorithm that snaps the position of one range image into great alignment to the other cloud. The implemented version follows the description of (Turk and Levoy, 1994):

1. Find the nearest position on mesh A to each point of mesh B;
2. Discard points out of range;
3. Delete pairs that are in a mesh boundary;
4. Find rigid transformation that minimizes weighting distance to the square minimum between the pairs of points.;
5. Run to converge;
6. Perform ICP on a more detailed mesh.

This ICP variant differs from classical ICP in several ways. First, a distance boundary was added to the nearest point to avoid combining any vertices B_i from a mesh to a remote part otherwise than corresponding to B_i. This vertex B_i of the mesh B may be a part of the scanned object that has been not captured in mesh A. In (Turk and Levoy, 1994), it is said that an excellent record is when the distance is adjusted to double the spacing between the reach points. Limiting the distance between pairs of corresponding points we performed step 2 (eliminating remote peers) while searching for closest points in step 1.

3.2 Random Sampling

Random sampling is a good downsampling technique, objectifying only to find internal points (Masuda et al., 1996). We apply this technique to a first image R^I, and we draw a set of N_S points of R^I randomly. One way to evaluate a probability of a good sampling and considering a random sampling from a probabilistic view point. Whatever epsilon a rejection of outliers by noise or occlusion, a probability of choice inliers is $1-\varepsilon$. In addition, a probability of choosing a subset with N_S points that are all inliers is $(1-\varepsilon)$. The N_T value is a hair probability minus a sub-sample being composed only of curious. The equation that governs this method is shown below:

$$p(\varepsilon, N_S, N_T) = 1-(1-(1-\varepsilon)^{N_S})^{N_T} \qquad (2)$$

An example of random sampling can be seen in (Nazem et al., 2014). In this paper, 70% of the data sets are sampled before the registration process.

4 CLOUD PARTITIONING ICP

In line with that, recently authors proposed the cloud partitioning approach to work prior the execution of the ICP algorithm (CP-ICP). In the present version of the algorithm, the idea behind the CP-ICP is to separate the whole point cloud into smaller groups (k groups in total) named hereafter subclouds, and then repeat the registration process for every subcloud until a stop criterion is found, as explained in section 4.1; by doing that, we considerably reduce the amount of computations because the point clouds are reduced in size.

Originally (Pereira et al., 2015), ,the implementation did not consider the existence of a stop criterion, what led to verification of k subclouds, and this sometimes proved to be unneccessary.The partitioning process decreases the amount of data to be processed by ICP in iteration, and the adoption of a stop criterion prevents the algorithm from having to align among all the subnets, stopping in the alignment of some subcloud that has a lower RMSE than the stopping criterion, which leads to time consuming and a guarantee of a quality registration, although, within the set of subnets there may be some where the alignment is even better and the RMSE measurement confers smaller values even of iteration where the algorithm converge. Cutting of the point clouds in the CP-ICP can be illustrated in Fig. 2, where after being identified where the cloud centroid is and its Z-axis, the cuts are done in subclouds.

To get a better view on the above claiming, let N_X and N_P be the size of two clouds undergoing registration by the ICP. The cost for the closest point computation in the classical ICP is $O(N_X N_P)$ (Besl and McKay, 1992), whereas using the partitioning into subclouds makes the cost of the closest point computation to range from $O(N_X N_P/k^2)$ to $kO(N_X N_P/k^2)$. This is because the stop criterion considered in the current version, illustrated in the diamond of the flowchart in Fig. 3 may interrupt the whole matching at any iteration from 1 to k.

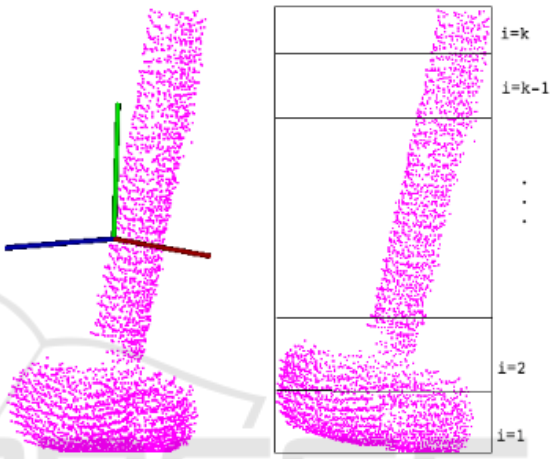

Figure 2: The left side the identification of each axis of the Hammer cloud in the coordinate system and to the right we have after the identification of Z, the cut in k sub-clouds.

4.1 Sufficient Registration

Consider two point clouds: an input point cloud and a target point cloud. The goal is to successfully perform a registration procedure, which means matching the input point cloud to the target one. To apply the CP-ICP method, we perform the following steps:

1. Subdivide each dataset (input and target) into k subclouds;
2. For each of the k iterations, solve the ICP algorithm for a pair of subclouds. The correspondence is checked between subclouds having the same index, and not one against all.

- Apply the achieved transformation to the initial input point cloud (named from now on input post ICP);
- The input post ICP is then compared to the target point cloud, using RMSE error at each iteration;
- If the RMSE value achieved in a given iteration is acceptable (stop criterion) the algorithm ends and the wanted registration is outcome. This is a decision step and, as such, represented by diamond in the flowchart of Fig. 3.

These steps are illustrated in the flow-chart of Fig. 3.

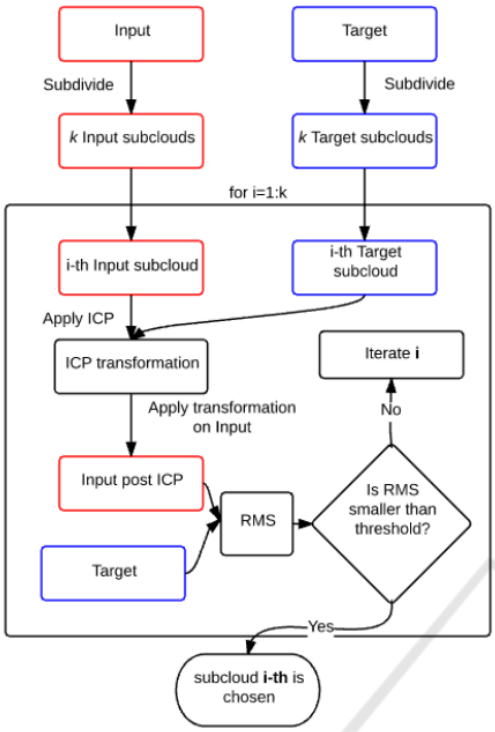

Figure 3: Fluxogram illustrating how the CP-ICP achieve a sufficient registration.

Adopting a stop criterion is useful because it limits the amount of correspondence checks between pairs of subclouds, thus avoiding unneccessary repetitions of ICP algorithm.

4.2 Tradeoff Between Solutions and Time

Considering the CP-ICP method as shown in 3, one can see that the more subclouds the more solutions for transformation matrices are obtained, which is good for finding an acceptable registration. However, time consumption rises accordingly, what is a drawback, and reveals a tradeoff between the number of solutions and the time consumption. That is why we added a stop criterior to this algorithm. By doing that at every correspondence check between pairs of subclouds, we give the algorithm the ability to escape and finish the matching whenever a good alignment is found. Although in the current version the stop criterion is determined a priori, this strategy has the advantage to help reducing computational cost (compared to the old published version).

To better explain the influence of the amount of subclouds into the timing performance, we studied the total elapsed time of the CP-ICP method, Fig. 4, as well as the time spent in a single iteration, Fig. 5, for different values of k. In figure 4 there are two curves; they correspond to two different choices for the step 2 of the algorithm in section 4.1. Once the indexation of the whole cloud and its grouping into k partitions is done, the user must choose between ascending or descending order to access the indexed subclouds in the search for the best one. In some examples of the database, the best subcloud is found near the beginning of the *for*-loop, whereas in other data it takes the whole spectrum of subclouds to be checked, slowing down the CP-ICP running time. These two limit cases are the ones represented by the lines of Fig. 4. In the example of the figure, the downward direction choice for accessing the i-th subcloud led to faster CP-ICP execution.

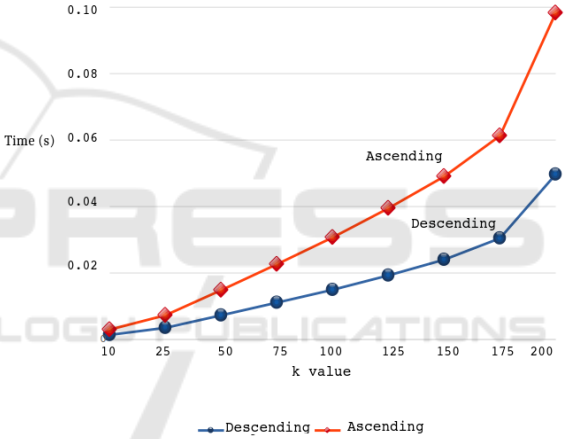

Figure 4: The full time consumption.

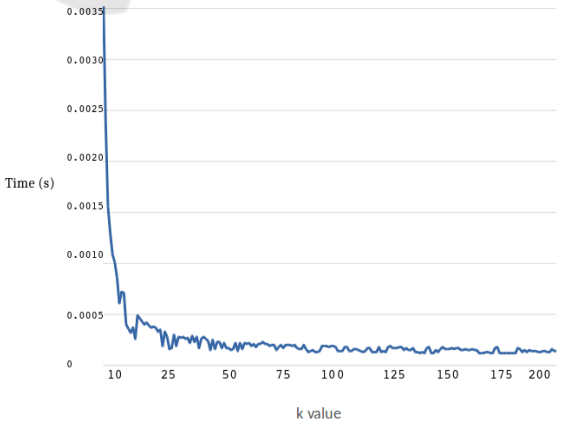

Figure 5: The time consumption for a single iteration for the Horse model.

5 MATERIALS AND METHODS

5.1 Available Datasets

The performance of the proposed CP-ICP method was evaluated from two different database. The first one is a private database kindly provided by prof. Aleotti in (Aleotti et al., 2014) and consists of point clouds of several objects acquired from a 6DOF robot arm (Comau SMART six) equipped with a two-finger parallel gripper (Schunk PG-70) and a high-resolution range laser scanner (SICK LMS 400), both mounted at the wrist of the robot arm. From this database we used two models in our experiments, namely the Horse and the Hammer models, illustrated in Fig. 6.

Figure 6: Objects from the database in (Aleotti et al., 2014). The Horse model (left) and Hammer (right).

The perspectives available of those objects are labeled according to the angle of acquisition from the sensor in the scene. For the Horse model we consider the perspectives of 0^o and 180^o. For the Hammer model we consider the perspectives of 0^o and 45^o. The second database is the Stanford 3D scanning repository, illustrated in (Curless and Levoy, 1996), which is a public database with several 3D models.

Figure 7: Objects from the database in (Curless and Levoy, 1996). The Dragon model (left) and Happy Buddha (right).

Similarly, the perspectives available of those objects are related to the acquisition angle.The image acquired from the zero degree perspective is taken as target cloud, whereas the one acquired from 24 degrees is considered as source cloud. Table 1.

Table 1: Various dataset size.

Number of points		
Cloud	Source	Target
Horse	3335	3298
Hammer	1852	2024
Dragon	41841	34836
Buddha	78056	75582

5.2 Methodology

As pointed out earlier, the goal of this paper is to introduce a new sampling method prior the ICP algorithm (CP-ICP). To evaluate how it performs, we compare CP-ICP with random sampling methods (keeping up to 50% and 70% of the original point cloud size) and also with a uniform sampling. In addition, we also considered the no-sampling case, which is the classical ICP method of (Besl and McKay, 1992) as implemented in PCL. The ICP algorithm then follows the sampling methods under study, and the quality of the 3D registration is evaluated through the Euler angles of the rotation matrix, by a metric based on root mean squared (RMSE) error and, finally, by another metric based on an adaptation of the structural similarity index (SSIM), to be discussed next. In Fig. 8, this process is summarized.

5.3 Metrics for Matching Evaluation

We have adopted three different metrics to evaluate the registration results and compare the sampling methods. The first one is based on the root mean squared error between the target point cloud and the input point cloud after proper rotation correction.

The RMSE eror can be calculated by the following formula:

$$RMSE = \sqrt{\frac{1}{N}\sum_{i=1}^{N}(\min_{x\in S} \parallel y_i - x \parallel_2)^2}, \qquad (3)$$

where S is an arbitrary surface and $y1,...,yN$ are coordinate points in $\Re^3$, representing the surface vertices or cloud points depending on a distance between two surfaces or between a surface and a point in the cloud.

The second metric is based on comparing the Euler angles from each transformation matrix obtained through ICP. This can only be done to the Dragon and Buddha models, since they have a ground truth.

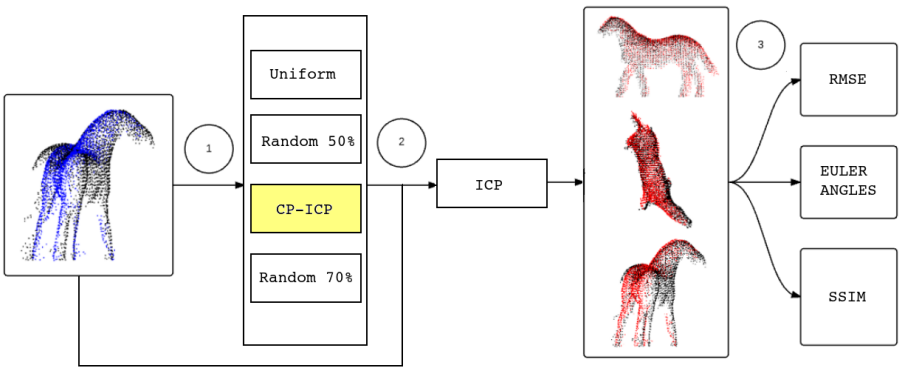

Figure 8: Methodology adopted to compare the sampling methods. In (1) the clouds go through a sampling process, in (2) the ICP is applied to perform the alignment, in (3) the outputs of the registry go through the evaluation of the registry quality metrics.

The rotation matrix can be defined by R, and the results of the Euler angles are obtained by the resolutions of the trigonometric products contained therein (Corke, 2017).

$$R = \begin{bmatrix} c_y c_z & c_x s_x s_y - c_x s_z & s_x s_z + c_x c_z s_y \\ c_y s_z & c_x c_z + s_x s_y s_z & c_x s_y s_z - c_z s_x \\ -s_y & c_y s_x & c_x c_y \end{bmatrix} \quad (4)$$

where: c_x=$cos(\alpha)$, c_y=$cos(\beta)$, c_z=$cos(\gamma)$, s_x=$sen(\alpha)$, s_y=$sen(\beta)$ and s_z=$sen(\gamma)$.

The last metric is based on the SSIM index, which is a traditional approach to measure image quality. It is also a method applied to identify similarity between two gray-scale images, where one of them is treated as a reference image. The SSIM index is an image quality metric which assess three characteristics of an image: the contrast, luminance and structure, each of them being calculated from statistical parameters of the input images.

In this paper, we adapt a method which uses the SSIM index to perform the comparison between 3D models by creating 2D images of different perspectives of each model and comparing them using the SSIM index. To illustrate how the method is made suitable for 3D, we start with the registration result as obtained by the CP-ICP for the Horse model from five perspectives, in Fig. 9.

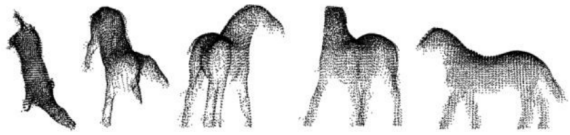

Figure 9: The five perspectives for the CP-ICP registration of the Horse model.

The use of the SSIM technique here relies on generating three images for each perspective: dot pattern image, full image and edge image, each one with 512x512 resolution. We got the dot pattern image after a quantization of point dataset as visualized from one of the perspectives, whereas the others are achieved from morphological transformations applied in the dot pattern image. Fig. 10(a), 10(b) and 10(c) show this set of images using as example the first perspective of 9. Fig. 10(b) and 10(c) are respectively the images after dilation and border extraction (Soille, 2003).

Dilation depicted in Fig.10(b) is the result of probing and expanding (until background is found) the inner of the input image from a structuring element. Border extraction then follows this dilation by means of subtracting it from the input image.

According to (Wang et al., 2004), the functions $l(a,b)$, $c(a,b)$ and $s(a,b)$ are then defined as:

$$l(a,b) = \frac{2\mu_a\mu_b + C_1}{\mu_a^2 + \mu_b^2 + C_1} | C_1 = (K_1 L)^2, K_1 \ll 1 \quad (5)$$

$$c(a,b) = \frac{2\sigma_a\sigma_b + C_2}{\sigma_a^2 + \sigma_b^2 + C_2} | C_2 = (K_2 L)^2, K_2 \ll 1 \quad (6)$$

$$s(a,b) = \frac{2\sigma_{ab} + C_3}{\sigma_a\sigma_b + C_3} | C_3 = (K_3 L)^2, K_3 \ll 1 \quad (7)$$

Where μ_a and μ_b are the pixel intensities of each image, σ_a and σ_b are the standard deviations, C_1, C_2 and C_3 are constants added to each term, L is the pixel range (255 for 8-bit grayscale images, e.g.) and K_1,K_2 and K_3 are constants less than unity. In addition, σ_{ab} is calculated as:

$$\sigma_{ab} = \frac{1}{N_a - 1} \sum_{i=1}^{N_a} (a_i - \mu_a)(b_i - \mu_b) \quad (8)$$

Finally, the metric takes the form presented below:

$$SSIM(a,b) = \frac{(2\mu_a\mu_b + C_1)(2\sigma_{ab} + C_2)}{(\mu_a^2 + \mu_b^2 + C_1)(\sigma_a^2 + \sigma_b^2 + C_2)} \quad (9)$$

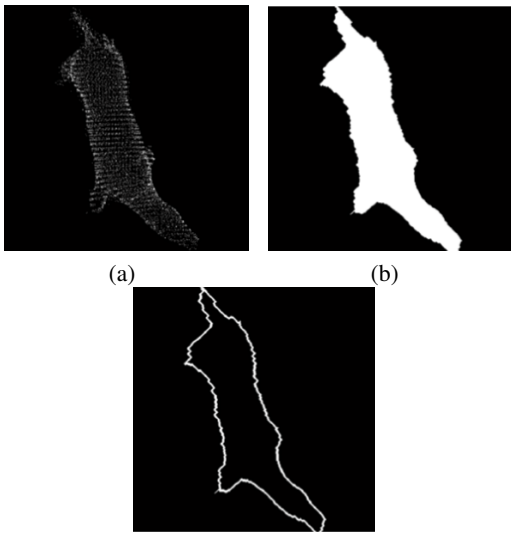

(a) (b)

(c)

Figure 10: The three kind of images generated for each perspective of each model. In (a) dot pattern image, in (b) full image (dilated), in (c) edge image (border extraction).

6 RESULTS

6.1 Elapsed Time

Table 2 synthetizes the time performance of the various sampling approaches; as it is clear from the results, the proposed CP-ICP sampling method achieved top performance for each 3D model studied. Such a good performance of the proposed approach somewhat confirms the expectations about the reduced computational efforts of the cloud matching algorithm, as mentioned in Section 4.

Table 2: Time comparision in seconds between sampling methods.

	Buddha	Dragon	Horse	Hammer
CP-ICP	**0.62**	**0.22**	**0.048**	**0.025**
ICP	17.68	7.40	0.41	0.37
Rnd. 50	17.85	4.01	0.36	0.19
Rnd. 70	18.72	5.82	0.43	0.26
Uniform	14.27	4.39	0.58	0.35

These numbers are impressive because they emphasize that the proposed approach is faster than the benchmark, and the impact into this particular research field is therefore evident.

6.2 RMSE Metrics

As explained earlier, in addition to the analysis of the performance regarding the time required to complete the registration procedure we also looked for a quantitative measure of the matching quality. In this paper we suggest to use, in a first moment, the root mean squared error between the target point cloud for the ICP algorithm and the input post ICP.

From Table 3, we can see that the CP-ICP method and the other approaches perform similarly. To illustrate with images what these numbers express, Fig. 11 brings the cloud matching for the Dragon model, which is a big-size point cloud. In Fig. 11(a) we can see the ICP registration (with no sampling), whereas the matching using the CP-ICP method is plotted in Fig. 11(b).

Table 3: RMSE evaluated after the ICP with each technique. The numbers are multiplied by 10^2.

10^{-2}	Buddha	Dragon	Horse	Hammer
CP-ICP	0.26	**0.18**	0.98	0.60
ICP	**0.24**	**0.18**	**0.97**	**0.57**
Rnd. 50	**0.24**	0.19	1.08	0.60
Rnd. 70	**0.24**	**0.18**	1.05	0.59
Uniform	**0.24**	0.19	**0.97**	0.58

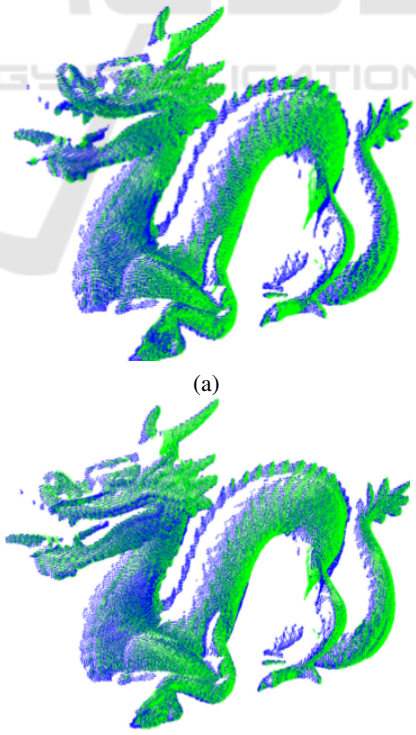

(a)

(b)

Figure 11: Registration results for the Dragon models. In a) the result obtained with the classical ICP In b) the CP-ICP.

6.3 Euler Angles Analysis

As an additional result for the quantitative analysis of the point cloud matching, in Table 4 and 5 the transformation matrix is represented by its Euler angles. The total error is the sum of the Z-, Y- and X- axis minus the ground-truth.

This was made only for the Dragon and Buddha models because the ground truth is known to be 24^o around Z axis.

Table 4: Euler angle of Happy Buddha model.

Buddha				
In degree	Z	Y	X	Total error
CP-ICP	**24.01**	**-0.13**	**-0.14**	**0.26**
ICP	18.98	0.54	-0.81	5.29
Rnd. 50	19.33	0.37	-0.82	5.12
Rnd. 70	19.13	0.42	-0.79	5.24
Uniform	19.11	0.30	-0.75	5.34

Table 5: Euler angle of Dragon model.

Dragon				
In degree	Z	Y	X	Total error
CP-ICP	23.77	**0.08**	0.24	**0.09**
ICP	**23.91**	0.16	**0.23**	0.30
Rnd. 50	23.88	0.14	0.23	0.25
Rnd. 70	23.89	0.17	0.24	0.30
Uniform	23.89	0.15	0.24	0.28

Once again, the CP-ICP was shown to be superior also from a quantitative point of view. The reader should especially note the column for the Z axis of the Buddha model. Besides that, we can observe the column representing the total error, which is the sum of the angles in the three axes: while the estimates from the other techniques deviate of about 5 degrees, the CP-ICP error approches zero. The success of the CP-ICP on finding the Euler angles which best represent the relative orientation between the point clouds relies on the fact that our algorithm is able to identify the region of the 3D model which preserves the most important points describing the rigid transformation searched. Unlike ICP, which searches for optimal transformation in the entire source cloud,

in CP-ICP this is done one sub-cloud at a time, in a ”light fashion.

6.4 SSIM-based Metrics

Tables 6 to 9 show the analysis of the five perspectives of each of the 3D models studied, using metrics based on SSIM, and represent average values between the perspectives. Tables 6 and 7 are related to the Buddha and Dragon models (largest data sets), while 8 and 9 are related to the Hammer and Horse models (small datasets). As shown in Tables 6 and 7, different to what has been seen so far, the various methods performs better in the Buddha model according to the proposed metrics. In the comparision between the sampling approaches, once again CP-ICP beats them all.

The results obtained for the evaluation through the SSIM can be seen in the tables below, with the best overall results, that is, the averages of all dot pattern, full and contour views highlighted in bold. It is seen that, in all cases, the best mean was CP-ICP.

Table 6: SSIM based comparison for the Happy Buddha model.

	Buddha			
	Dot	Full	Contour	Mean
CP-ICP	**0.884**	0.941	**0.982**	**0.936**
ICP	0.822	**0.947**	0.965	0.911
Rnd. 50	0.869	**0.947**	0.979	0.911
Rnd. 70	0.872	**0.947**	0.975	0.932
Uniform	0.876	0.953	0.975	0.935

Table 7: SSIM based comparison for the Dragon model.

	Dragon			
	Dot	Full	Contour	Mean
CP-ICP	0.568	**0.683**	**0.967**	**0.740**
ICP	0.570	0.621	0.900	0.697
Rnd. 50	**0.583**	0.644	0.902	0.716
Rnd. 70	0.570	0.621	0.902	0.698
Uniform	0.576	0.632	0.916	0.708

Table 8: SSIM based comparison for the Hammer model.

	Hammer			
	Dot	Full	Contour	Mean
CP-ICP	**0.962**	0.936	**0.999**	**0.966**
ICP	0.931	0.921	**0.999**	0.950
Rnd. 50	0.940	0.935	0.998	0.958
Rnd. 70	0.938	0.934	**0.999**	0.957
Uniform	0.941	**0.938**	0.992	0.960

Table 9: SSIM based comparison for the Horse model.

	Horse			
	Dot	Full	Contour	Mean
CP-ICP	**0.902**	0887	**0.999**	**0.929**
ICP	0.901	0.889	0.996	**0.929**
Rnd. 50	0.892	**0.891**	**0.999**	0.928
Rnd. 70	0.892	0.843	**0.999**	0.928
Uniform	0.891	0.889	**0.999**	0.926

In general, for the four point cloud models used, the SSIM metrics agrees with the other ones and confirms the superior matching quality of the CP-ICP.

Overall, these tables and figures reveal that the CP-ICP approach presented the best performance for all point cloud models.

For the sake of illustration, Fig. 12 brings the registration results: a)using the CP-ICP; b) using random sampling with 70% of the points and c) using the ICP with no sampling. The highlighted regions of 12(a) reveals that the registration following cloud partitioning approach achieved a better qualitative result, though quantitatively the ICP method softly beat it (see Table 3).

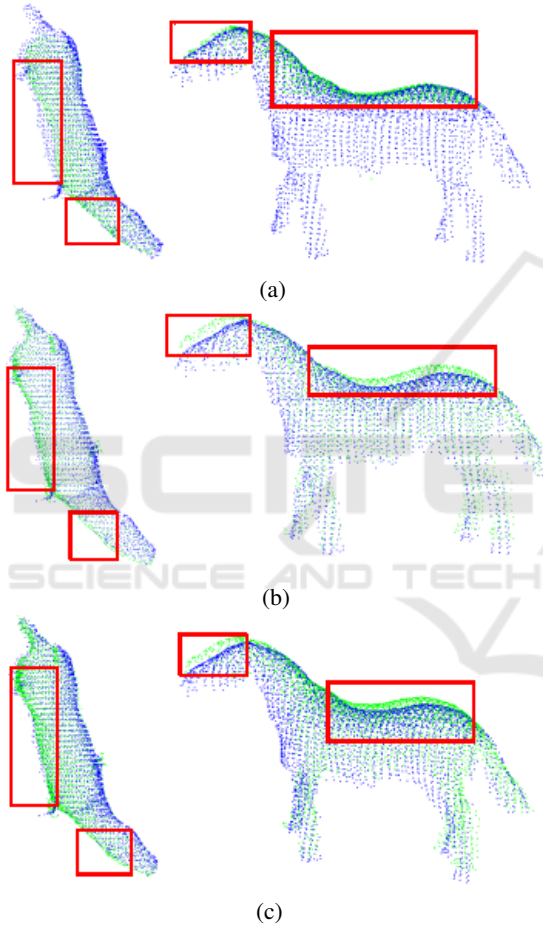

(a)

(b)

(c)

Figure 12: Comparison of the registration results for the Horse model. In a) the registration for the CP-ICP b) the registration result for the random 70% sampling and in c) the registration result for the ICP with no samling.

Finally, in Fig. 13 the registration results for the Buddha are plotted. For the Buddha model, we can clearly see that the CP-ICP result presents itself as the best registration, as denoted in the marked regions in 13(f)

7 ROBUSTNESS TO NOISE AND OCCLUSION

In (Masuda and Yokoya, 1995), a robust noise and occlusion technique is discussed, which motivated experiments to test the robustness of our technique. To accomplish with that, we considered adding gaussian noise and subjecting the clouds to occlusion. Only the Buddha and Dragon models were considered here. The probability density function p of a Gaussian random variable z is given by:

$$p_G(z) = \frac{1}{\sqrt{\sigma * 2\pi}} e^{\frac{-(z-\mu)^2}{2\sigma^2}} \tag{10}$$

where z represents the grey level, μ the mean value and σ the standard deviation. In this case $\sigma = 0.001$.

The results are summarized in Tables 10 and 11, which bring the various metric adopted and the different sampling approaches at a glance. We can observe the best performance is achieved by CP-ICP, which approached better the 24 degrees Z-axis rotation of the ground truth in extremely short time. Errors regarding the other axis follow analogously and are omitted for brevity. In addition to the observation of the tables, we can make a brief visual inspection in Fig. 14(e), looking at the Buddha's feet. We can say that the regions between the clouds of origin and target overlap perfectly when registration follows CP-ICP.

Table 10: Table with comparison metrics for the Buddha model for registration with Gaussian noise addition.

Buddha				
	Time (s)	RMSE	Angle (^{o})	SSIM
CP-ICP	**0.67**	**0.19**	**21.30**	**0.901**
ICP	15.32	0.21	15.71	0.897
Rnd.50	7.44	021	16.02	0.889
Rnd.70	10.71	0.20	16.00	0.888
Uniform	10.62	0.20	16.01	0.889

Table 11: Table with comparison metrics for the Dragon model for registration with Gaussian noise addition.

Dragon				
	Time (s)	RMSE	Angle (^{o})	SSIM
CP-ICP	**0.18**	**0.16**	**23.97**	**0.778**
ICP	7.03	0.17	23.59	0.769
Rnd.50	4.17	0.18	23.59	0.765
Rnd.70	5.58	0.17	23.58	0.769
Uniform	4.12	0.18	23.58	0.756

The robustness to occlusion was studied from the Horse model. One of the main problems of projecting the 3D scene to the image plane is occlusion - each object blocks the view of others behind it (Huang

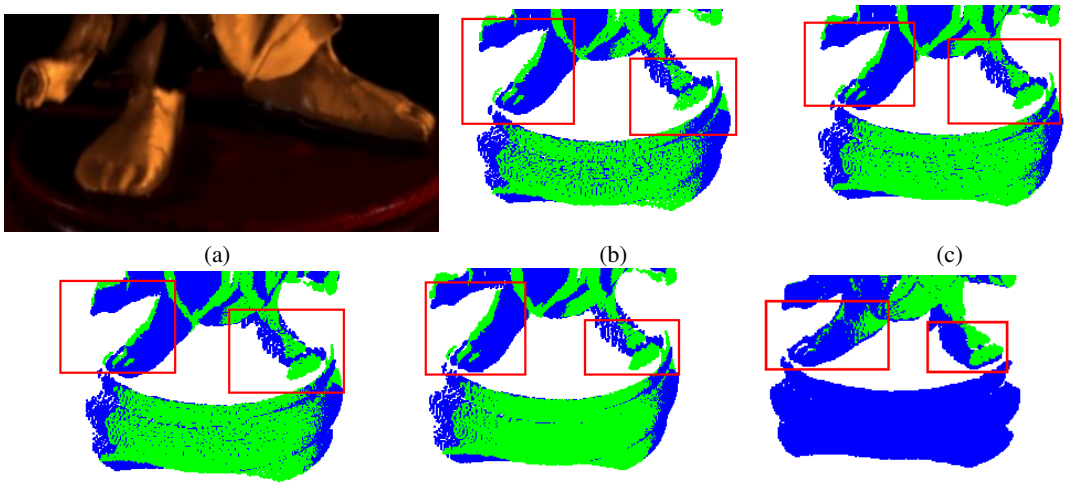

(a) (b) (c)

(d) (e) (f)

Figure 13: Comparison of the registration results for the Buddha model. In a) the image of the foot of the Buddha, in b)the registration result for the random 50% sampling and in c) the registration result for the random 70% sampling and in d) the registration result for the uniform sampling and in e) the registration result for the ICP with no samling and finally in f)the registration result of use CP-ICP method.

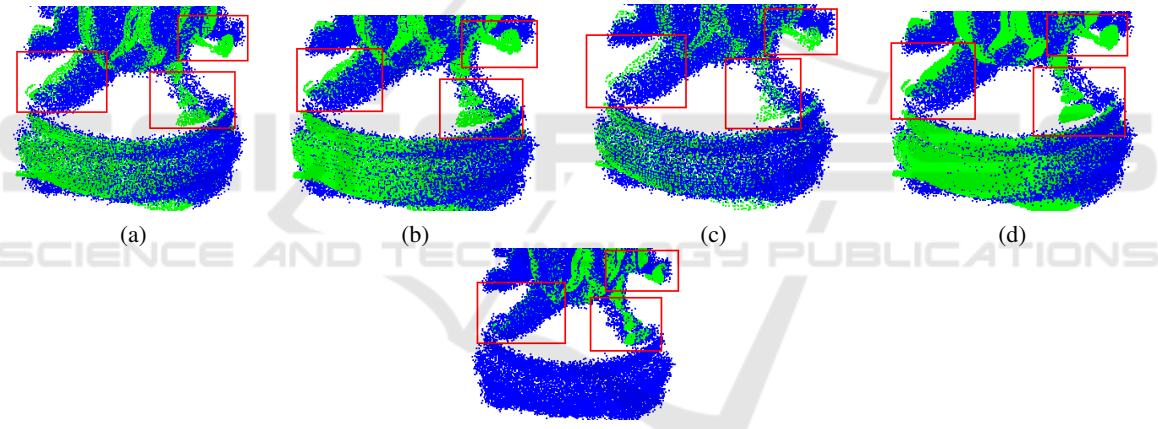

(a) (b) (c) (d)

(e)

Figure 14: Comparison of registration results for the Buddha model with Gaussian noise of standard deviation 0.001. In a) the registration result for the random 50% sampling and in b) the registration result for the random 70% sampling and in c) the registration result for the uniform sampling and in d) the registration result for the ICP with no samling and finally in e)the registration result of use CP-ICP method.

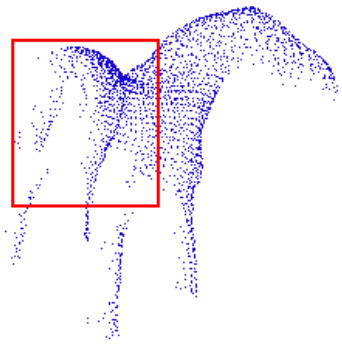

Figure 15: Horse model occluded.

et al., 2017). The occlusion can be caused by the omission of the vision of a given mass of points due to the presence of another object in the front, or can be caused by a rotation of the object itself. For the latter case, we call it self-occlusion.

In our experiment, a local maximum filter of the PCL itself was used to make localized removal of points in the back of the Horse, causing the lateral points at left to disappear almost completely. The sketch of it can be seen in Fig. 15. Despite of that image perturbation, CP-ICP outperformed the various sampling methods.

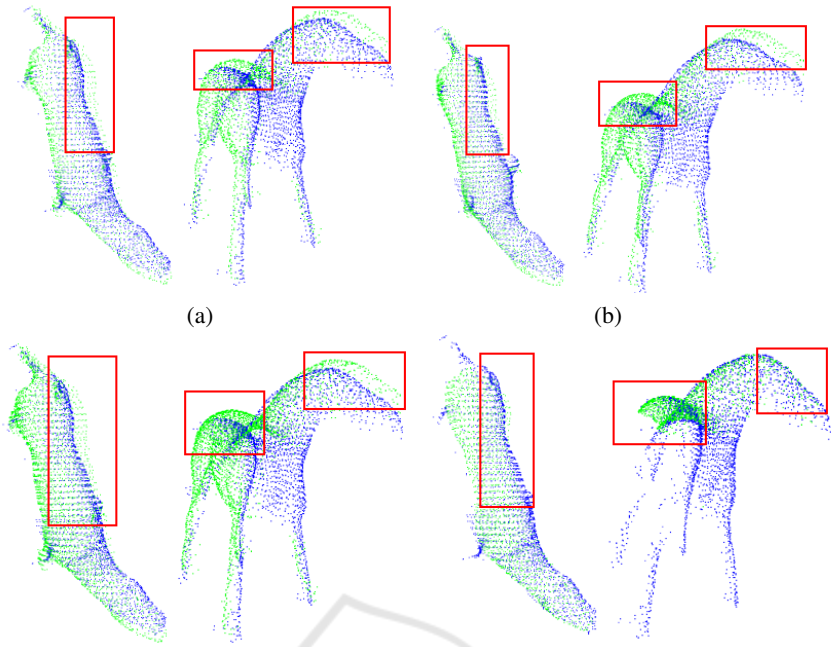

Figure 16: Results for the Horse model with partial occlusion of points. In a) the registration result for the random 50% sampling and in b) the registration result for the random 70% sampling and in c) the registration result for the ICP with no samling and finally in e)the registration result of use CP-ICP method.

Table 12: Results of registration of Horse model apllying occlusion.

Horse				
	Time (s)	RMSE	Angle	SSIM
CP-ICP	**0.052**	1.37	**180.00**	**0.943**
ICP	0.94	**1.32**	177.56	0.939
Rnd.50	0.53	1.42	177.17	0.940
Rnd.70	0.74	1.41	177.34	**0.943**

Observing the result in the table 12, the register with the CP-ICP presents better results: it completely found the ground truth and, in addition, reached the highest SSIM. For what concerns the RMSE measure, it fluctuated very little amongst the sampling methods and, hence, it can't be used as a faithful comparison metric in these cases.

Robustness of CP-ICP to added noise is related to its ability to keep the original data of the point clouds; indeed, not even a single point is lost when sub-clouds are checked for correspondence. Unlikely, sampling approaches lead to loss of input data (in some case it leads to pseudodata generation), and consequently noise gets more important, thus biasing the ICP to find erroneous correspondences.The success of the CP-ICP technique when dealing with self-occlusion may be associated to the partitioning itself: since we search for correspondences between sub-clouds, even under partial occlusion scenario there are many sub-clouds in which the input data is fully preserved and, as such, are useful for correspondence search.

8 CONCLUSIONS

In this paper, a pre-processing method was presented for registration along with ICP. The method is compared with other four techniques using an RMSE metric, Euler angles, and one metric adapted from SSIM. The results show that, in comparison to the other methods, author's approach provided a better registration in shorter times. This technique also presented robustness to data corruption by gaussian noise and subject to occlusion, as well. This is therefore, a promising and useful preprocessing step to use with ICP variants in real time applications of 3D modelling.As future work, we will make the algorithm fully automatic, as well we will implement the alignment of one sub-cloud against all.

ACKNOWLEDGEMENTS

The authors are grateful to Professor Marques for lab facilities and agency FUNCAP for the financial support.

REFERENCES

Aleotti, J., Rizzini, D. L., and Caselli, S. (2014). Perception and grasping of object parts from active robot exploration. *Journal of Intelligent & Robotic Systems*, 76(3-4):401–425.

Besl, P. J. and McKay, N. D. (1992). Method for registration of 3-d shapes. In *Sensor Fusion IV: Control Paradigms and Data Structures*, volume 1611, pages 586–607. International Society for Optics and Photonics.

Ćesić, J., Marković, I., Jurić-Kavelj, S., and Petrović, I. (2016). Short-term map based detection and tracking of moving objects with 3d laser on a vehicle. In *Informatics in Control, Automation and Robotics*, pages 205–222. Springer.

Chaudhury, A., Ward, C., Talasaz, A., Ivanov, A. G., Huner, N. P., Grodzinski, B., Patel, R. V., and Barron, J. L. (2015). Computer vision based autonomous robotic system for 3d plant growth measurement. In *Computer and Robot Vision (CRV), 2015 12th Conference on*, pages 290–296. IEEE.

Cigla, C., Brockers, R., and Matthies, L. (2017). Image-based visual perception and representation for collision avoidance. In *IEEE International Conference on Computer Vision and Pattern Recognition, Embedded Vision Workshop*.

Corke, P. (2017). *Robotics, Vision and Control: Fundamental Algorithms In MATLAB® Second, Completely Revised*, volume 118. Springer.

Curless, B. and Levoy, M. (1996). A volumetric method for building complex models from range images. In *Proceedings of the 23rd annual conference on Computer graphics and interactive techniques*, pages 303–312. ACM.

Gorecky, D., Schmitt, M., Loskyll, M., and Zühlke, D. (2014). Human-machine-interaction in the industry 4.0 era. In *Industrial Informatics (INDIN), 2014 12th IEEE International Conference on*, pages 289–294. IEEE.

Holz, D., Ichim, A. E., Tombari, F., Rusu, R. B., and Behnke, S. (2015). Registration with the point cloud library: A modular framework for aligning in 3-d. *IEEE Robotics & Automation Magazine*, 22(4):110–124.

Huang, P., Cheng, M., Chen, Y., Luo, H., Wang, C., and Li, J. (2017). Traffic sign occlusion detection using mobile laser scanning point clouds. *IEEE Transactions on Intelligent Transportation Systems*, 18(9):2364–2376.

Malamas, E. N., Petrakis, E. G., Zervakis, M., Petit, L., and Legat, J.-D. (2003). A survey on industrial vision systems, applications and tools. *Image and vision computing*, 21(2):171–188.

Masuda, T., Sakaue, K., and Yokoya, N. (1996). Registration and integration of multiple range images for 3-d model construction. In *Pattern Recognition, 1996., Proceedings of the 13th International Conference on*, volume 1, pages 879–883. IEEE.

Masuda, T. and Yokoya, N. (1995). A robust method for registration and segmentation of multiple range images. *Computer vision and image understanding*, 61(3):295–307.

Nazem, F., Ahmadian, A., Seraj, N. D., and Giti, M. (2014). Two-stage point-based registration method between ultrasound and ct imaging of the liver based on icp and unscented kalman filter: a phantom study. *International journal of computer assisted radiology and surgery*, 9(1):39–48.

Pan, J., Chitta, S., and Manocha, D. (2017). Probabilistic collision detection between noisy point clouds using robust classification. In *Robotics Research*, pages 77–94. Springer.

Pereira, N. S., Carvalho, C. R., and Thé, G. A. (2015). Point cloud partitioning approach for icp improvement. In *Automation and Computing (ICAC), 2015 21st International Conference on*, pages 1–5. IEEE.

Rodolà, E., Albarelli, A., Cremers, D., and Torsello, A. (2015). A simple and effective relevance-based point sampling for 3d shapes. *Pattern Recognition Letters*, 59:41–47.

Rusinkiewicz, S. and Levoy, M. (2001). Efficient variants of the icp algorithm. In *3-D Digital Imaging and Modeling, 2001. Proceedings. Third International Conference on*, pages 145–152. IEEE.

Soille, P. (2003). *Morphological image analysis: principles and applications*. Springer Science & Business Media.

Toro, C., Barandiaran, I., and Posada, J. (2015). A perspective on knowledge based and intelligent systems implementation in industrie 4.0. *Procedia Computer Science*, 60:362–370.

Turk, G. and Levoy, M. (1994). Zippered polygon meshes from range images. In *Proceedings of the 21st annual conference on Computer graphics and interactive techniques*, pages 311–318. ACM.

Wang, Z., Bovik, A. C., Sheikh, H. R., and Simoncelli, E. P. (2004). Image quality assessment: from error visibility to structural similarity. *IEEE transactions on image processing*, 13(4):600–612.

Weinmann, M. (2016). Outlier removal and fine registration. In *Reconstruction and Analysis of 3D Scenes*, pages 84–85. Springer.

Zhang, J. and Lin, X. (2017). Advances in fusion of optical imagery and lidar point cloud applied to photogrammetry and remote sensing. *International Journal of Image and Data Fusion*, 8(1):1–31.